2015

Change in chirality of semiconducting single-walled carbon nanotubes can overcome anionic surfactant stabilisation: a systematic study of aggregation kinetics

Iftheker A. Khan
University of Rhode Island

Joseph R. V. Flora

See next page for additional authors

Citation/Publisher Attribution
Khan Iftheker A., Flora Joseph R. V., Afrooz A. R. M. Nabiul, Aich Nirupam, Schierz P. Ariette, Ferguson P. Lee, Sabo-Attwood Tara, Saleh Navid B. (2015) Change in chirality of semiconducting single-walled carbon nanotubes can overcome anionic surfactant stabilisation: a systematic study of aggregation kinetics. *Environmental Chemistry* **12**, 652-661.
Available at: https://doi.org/10.1071/EN14176

HHS Public Access

Author manuscript

Environ Chem. Author manuscript; available in PMC 2016 February 05.

Published in final edited form as:

Environ Chem. 2015 May 20; 12(6): 652–661. doi:10.1071/EN14176.

Change in Chirality of Semiconducting Single-Walled Carbon Nanotubes Can Overcome Anionic Surfactant Stabilization: A Systematic Study of Aggregation Kinetics

Iftheker A. Khan[1], **Joseph R. V. Flora**[2], **A. R. M. Nabiul Afrooz**[3], **Nirupam Aich**[3], **P. Ariette Schierz**[3], **P. Lee Ferguson**[4], **Tara Sabo-Attwood**[5], and **Navid B. Saleh**[3,*]

[1]Department of Chemical Engineering, University of Rhode Island, Kingston, RI 02881, USA

[2]Department of Civil and Environmental Engineering, University of South Carolina, Columbia, SC 29208, USA

[3]Department of Civil, Architectural, and Environmental Engineering, University of Texas, Austin, TX 78712, USA

[4]Department of Civil and Environmental Engineering, Duke University, Durham, NC 27708, USA

[5]Department of Environmental and Global Health, University of Florida, Gainesville, FL 32610, USA

Abstract

Single-walled carbon nanotubes' (SWNT) effectiveness in applications is enhanced by debundling or stabilization. Anionic surfactants are known to effectively stabilize SWNTs. However, the role of specific chirality on surfactant-stabilized SWNT aggregation has not been studied to date. The aggregation behavior of chirally enriched (6,5) and (7,6) semiconducting SWNTs, functionalized with three anionic surfactants—sodium dodecyl sulfate (SDS), sodium dodecyl benzene sulfonate (SDBS), and sodium deoxycholate (SDOCO)—was evaluated with time-resolved dynamic light scattering. A wide range of mono- (NaCl) and di-valent ($CaCl_2$) electrolytes as well as a 2.5 mg TOC/L Suwannee River humic acid (SRHA) were used as background chemistry. Overall, SDBS showed the most effectiveness in SWNT stability, followed by SDOCO and SDS. However, the relatively larger diameter (7,6) chiral tubes compromised the surfactant stability, compared to (6,5) chiral enrichment, due to enhanced van der Waals interaction. The presence of di-valent electrolytes overshadowed the chirality effects and resulted in similar aggregation behavior for both the SWNT samples. Molecular modeling results enumerated key differences in surfactant conformation on SWNT surfaces and identified interaction energy changes between the two chiralities to delineate aggregation mechanisms. The stability of SWNTs increased in the presence

*Corresponding author: Navid B. Saleh, navid.saleh@utexas.edu, Phone: (512) 471-9175.

Supporting Information

Table S1 shows the properties of surfactants used. Table S2 lists the mass concentration of surfactant-modified SWNTs. Table S3 lists the calculated D/G ratio from the Raman spectra. Table S4 reports the initial aggregation rate in the presence and absence of SRHA. Figure S1 shows representative chirality chart of SWNTs. Figure S2 provides AFM images. Figure S3 shows the diameter distributions of pristine SWNTs. Figure S4 reports the Raman spectra of SWNTs. Figure S5 shows EPM plots for SG76 SWNTs. Figures S6–S8 show the aggregation profiles of SWNTs with NaCl and $CaCl_2$. Figure S9 shows the intial aggregation rate in the presence and absence of SRHA. The supporting material is available online free of charge at the Environmental Chemistry journal homepage.

of SRHA under 10 mM monovalent and mixed electrolyte conditions. The results suggest that change in chirality can overcome surfactant stabilization of semiconducting SWNTs. SWNT stability can also be strongly influenced by the anionic surfactant structure.

Keywords

Chirality; single-walled carbon nanotube; anionic surfactants; aggregation kinetics; stability; molecular dynamic simulation

1. INTRODUCTION

A graphene sheet, rolled with respect to a principal axis in a specific rollover vector, forms a tubular structure known as a single-walled carbon nanotube (SWNT).[1] The atomic arrangements of the carbon atoms during this rolling-up process result in unique transverse structures denoted by chiral indices *n* and *m*.[2] Such unique helicity of SWNTs, as defined by chirality, causes variation in wave-function boundaries that represent the electron system of each carbon atom and alters the electronic structure for each specific chirality of SWNTs.[2, 3] The orientational uniqueness of SWNTs also results in novel mechanical, electrical, and optical properties, encouraging further studies in device and process applications.[4, 5] However, the bundling and aggregation propensity of SWNTs limit their effective use in applications.[6] Such limitations encouraged surface functionalization of SWNTs, both covalently[7] and non-covalently,[8] and thus widened the application premise. Well-dispersed SWNTs have been effectively incorporated into a variety of applications, including electronic devices,[4, 9] biophysical processing schemes and biomedical applications (i.e., drug delivery and imaging),[10] optical sensors,[11] membranes for water purification,[12] and nanocomposites.[13] The applied field has also caused a large market transfer of SWNTs, with immediate consequences in terms of environmental release and exposure.[14] The increased manufacturing and widened market share necessitate reliable prediction of SWNT fate and transport, not only in terms of key environmental parameters but more so in systematically evaluating the role of atomic properties and surface functionalities in their aquatic behavior.

High surface interaction (originating from van der Waals energy) in SWNTs can create bundled and aggregated structures in aqueous media.[15] Debundling and disaggregation can be achieved either with functionalization at the defective sites formed during synthesis, or using post-synthesis covalent and non-covalent surface treatments.[6] Covalent functionalization is achieved through sp^3 hybridization of defects and carboxyl group incorporation via oxidation, both in the sidewalls and open ends of the graphitic tubes.[16] Though such covalent functionalization schemes can cause effective debundling, breaking the C-C bond structure through the use of strong oxidants is known to compromise fundamental optical and electrical properties of the helicoids.[6] As an alternate to damaging surface oxidation, non-covalent functionalization results in effective dispersion without compromising novel surface properties.[17, 18] Such surface modification is typically achieved using natural polyelectrolytes (e.g., sodium lingnosulfonate, humic acid, fulvic acid, etc.),[19, 20] synthetic polymers,[21] organic solvents,[22] biomacromolecules,[8] and short-chained surfactants.[18, 23] Typically, long-chained organic molecules with strong

hydrophobicity or short-chained organics with aromatic structures adsorb onto SWNT surfaces. The developed soft outer shells essentially provide tube-tube repulsion, causing effective dispersion in aquatic media.[23] However, it is also known that change in the chirality of SWNTs can alter tube-tube interaction and thus can compromise the effectiveness of surfactant stabilization.

Extensive literature has been established on the stability behavior of different carbon allotropes; specifically, the behavior of fullerenes,[24, 25] covalently functionalized multiwalled carbon nanotubes (MWNTs),[26, 27] and covalently functionalized SWNTs.[28, 29] Key parameters evaluated include the effect of solubilization techniques for fullerenes,[24] the extent of oxidation for MWNTs,[27] and the effects of biomacromolecules on SWNTs.[28] Recently, the role of atomic arrangement or chirality of semiconducting SWNTs on their aggregation kinetics has also been systematically evaluated in one of our studies.[30] Moreover, extensive work has also been done to disperse SWNTs with anionic, cationic, and zwitterionic surfactant molecules.[8, 18, 23, 31, 32] Amphiphilic surfactants that are used to functionalize SWNTs or that pre-exist in natural systems have also shown to influence SWNT aggregation; e.g., two recent environmental fate and transport studies have evaluated sodium dodecyl sulfate (SDS)[31] and sodium dodecyl benzene sulfonate (SDBS)[32] in aqueous stabilization of SWNTs. The key findings here show the stability responses of SWNTs, modified with SDS and SDBS, for a range of background electrolyte conditions. Though the literature provides evidence of chirality's role in aggregation and attests to variation in stability by surfactant type, the chiral influences on the surfactant stabilization of SWNTs remain to be systematically studied, particularly while considering the distinct structure of surfactants.

The objective of this study is to evaluate the roles of chirality and surfactant structures in the aggregation behavior of SWNTs that have been modified with commonly used anionic surfactants. Furthermore, molecular modeling of SWNT-surfactant interaction is performed to delineate aggregation mechanisms. The surfactants considered include SDS, SDBS, and sodium deoxycholate (SDOCO). The presence of an aromatic ring differentiates SDBS from SDS, which will allow investigation of the effect of π-π interaction on SWNT aggregation. SDOCO, a commonly used surfactant for non-covalent SWNT functionalization, possesses a curved, cupped structure and thus will likely manifest unique chirality-dependent interaction. Detailed physicochemical and electrokinetic characterizations are performed using Raman spectroscopy, transmission electron microscopy (TEM), and electrophoretic mobility (EPM) measurements. Time-resolved dynamic light scattering (TRDLS) technique is used to study aggregation kinetics in a wide range of mono- and di-valent electrolyte conditions. Suwannee River humic acid (SRHA) is used to study the role of natural organic matter (NOM). A combination of electrokinetic properties, physicochemical characteristics, established macromolecule sorption literature, and high-performance molecular modeling data are utilized to enumerate aggregation mechanisms.

2. MATERIALS AND METHODS

2.1. Materials

CoMoCat SWNTs, SG65 (lot no. 000-0031) and SG76 (lot no. 0020), were procured from SouthWest NanoTechnologies Inc. (SWeNT, Norman, OK, USA). Independent characterization was performed earlier to confirm chiral specificity.[30] In brief, SG65 and SG76 have (6,5) and (7,6) chiral enrichment, respectively. In addition, other chiralities are present in minor quantities in SG65 and SG76 samples, which include (7,3), (7,5), and (8,4) for SG65 and (7,5), (7,6), (9,4),(10,3), and (12,1) for SG76 SWNTs. It is important to note that these are currently the only two specific chiral SWNT samples available commercially. Three anionic surfactants —SDS (10% solution), SDBS, and SDOCO—were obtained from Invitrogen, ACROS Organics, and Sigma Aldrich, respectively. The surfactant properties are listed in Table S1.

2.2. Functionalization of SWNTs

Surfactant stock solutions (0.02 %w/v) were prepared in deionized water (resistivity ~18.2 MΩ-cm) with each surfactant. SWNTs were added to surfactant stock (50 mL) to yield 105±5 mg/L initial concentration; i.e., a SWNT:surfactant ratio of 1:2. The solution was placed in an ice bath and then subjected to tip sonication (using a tapered 3.2 mm microtip horn and Misonix S-4000 sonicator; Misonix Inc., Farmingdale, NY) for 30 min (at 50 amplitudes). The sonication was performed in the ice bath to keep the temperature constant. An average energy input of 45±5 kJ was maintained for all samples. The dispersion was allowed to quiescently stand for 24 h and then subjected to centrifugation for 1 h at ~10,900 × g (Sorvall RC 5C plus, Thermo-Fisher, MA, USA). The supernatant was decanted to obtain stable surfactant-modified SWNT suspension, which served as stock for all subsequent measurements. The mass concentration of SWNTs solution at each stage, (i.e., right after sonication, after 24 h equilibration period, and upon centrifugation, as listed in Table S2) was measured with UV-Vis (Agilent 8453) spectroscopy at 570 nm and 655 nm wavelengths for SG65 and SG76, respectively.

2.3. Characterization of SWNTs

Atomic force microscopy (AFM), TEM, Raman Spectroscopy, and EPM measurements were performed to characterize SWNT samples. The details of the AFM protocol is provided in the supporting information. The TEM imaging followed the established protocol.[26, 28] Essentially, a drop of SWNT suspension was placed on a 200 mesh copper TEM grid (Ted Pella Inc.) and was allowed to dry (at 75 °C) for 15 min. Images were collected with an H-9500 (300 kV) TEM (Hitachi High Technologies America, Inc., CA) following random grid location selection. To evaluate the state of surface defects, Raman spectra were recorded with dry SWNT powders placed on glass slides and evaluated with LabRam confocal Raman spectrophotometer (JY Horiba, HORIBA Instruments, Irvine, CA), equipped with an He/Ne (632.817 nm) laser. Each spectrum presented is the average of at least five scans with integration times of 120 s. For electrokinetic characterization, EPM was measured with a Malvern Zetasizer (ZEN 3660) at 20 °C using the established protocol.[26, 28] In short, diluted stock solution (~1 mg/L) was used with relevant electrolytes and at least three replicates with 10 measurements were recorded.

2.4. Solution Chemistry

SWNT aggregation was initiated with the addition of mono- and di-valent electrolytes under environmentally relevant conditions: i.e., 0.1–1000.0 mM NaCl and 0.03–55.0 mM $CaCl_2$. The role of natural organic matter (NOM) was evaluated using 2.5 mg TOC/L Standard II Suwannee River humic acid, SRHA (International Humic Substances Society, Denver, CO) under 10 mM ionic strength (i.e., 10 mM NaCl and 7 mM NaCl with 1 mM $CaCl_2$).

2.5. Aggregation Kinetics Measurements

The aggregation kinetics of SWNTs was studied with an ALV/CGS-3 precision goniometer system (ALV-GmbH, Langen, Germany), equipped with a 22 mW He-Ne laser (632.8 nm wavelength). For the dynamic light scattering (DLS) studies, SWNTs (2 mL; ~1 mg/L) were added to pre-cleaned disposable borosilicate glass vials (Fisher Scientific, PA) that were soaked in cleaning solution (2%; Extran MA01, EMD Chemicals, NJ), and thoroughly rinsed with deionized water and oven-dried (Fisher Scientific, Pittsburg, PA) under dust-free conditions.[28, 30] Salt solutions at appropriate dilutions were added to initiate aggregation and the He-Ne laser was guided toward the sample, placed in a toluene-filled refractive index-matched vat. The scattered light intensity was detected at 90° with a photon counting module operating at 1.2 amperes and 5 volts (Perkin Elmer, Dumberry, Canada). The hydrodynamic radii of the particle clusters were estimated through second-order cumulant analysis (ALV software) and the average hydrodynamic radius (R_0) was calculated every 15 s, then corrected by an autocorrelation function for at least 30 min for each condition. Analysis of the DLS data included initial aggregate rate calculations for up to 1.3 times the initial hydrodynamic radius size, R_0. The rate of aggregation is known to be proportional to the rate of change of R_0 with time and can be expressed as follows (Equation 1);[28]

$$k \propto \frac{1}{N}\left[\frac{dR_0(t)}{dt}\right]_{\{t\to 0\}} \quad (1)$$

where, k is the initial aggregation rate, and N is the SWNT particle concentration.

To eliminate the influence of particle concentration, which can vary between samples, a normalized unit less quantity, known as attachment efficiency (α) is determined from the ratio of initial aggregation rate at each electrolyte condition with that of the favorable aggregation condition. Attachment efficiency 'α' is represented using Equation 2 as follows:[28]

$$\alpha = \frac{\left[\frac{dR_0(t)}{dt}\right]_{\{t\to 0\}}}{\left[\frac{dR_0(t)}{dt}\right]^{fav}_{\{t\to 0\}}} \quad (2)$$

where, α is the attachment efficiency, and *t* is the time of aggregation. All DLS measurements were conducted at 20±0.5 °C and at least 2 duplicate samples were tested to obtain significant reproducibility.

2.6. Molecular Modeling

The optimized geometries and binding energies of the surfactants on SWNTs in the gas phase were calculated using procedures adapted from Zaib et al.[33] The initial geometry of a repeating unit of a SWNT molecule with a chirality of SG65 and SG76 was obtained using a nanotube builder, Visual Molecular Dynamics (VMD) program. The ends of SWNTs were terminated with H atoms, and the resulting molecular formula was $C_{508}H_{26}$ and $C_{364}H_{22}$ for SG76 and SG65, respectively. The coordinates of the SWNTs and surfactant molecules were optimized with dispersion-corrected Density Functional Theory (DFT) using the BLYP functional and the 6-31G basis set as implemented in TeraChem.[34, 35]

To obtain the minimum energy configuration of the surfactants on the surface of the SWNTs, an estimate of the initial geometry was obtained by optimizing the surfactant on a SWNT fragment using their effective fragment potentials (EFP2) generated using General Atomic and Molecular Electronic Structure Systems, GAMESS.[36–39] A C_{54} fragment was cut out from the center of the SWNTs and the external carbons were terminated with H atoms. The H positions were then optimized at the DFT-D3/BLYP/6-31G level while keeping the C atoms fixed. The SWNT fragments and surfactants were re-oriented along their principal axes using MacMolPlt[40] and their EFP2 were generated at the 6-31G level using numerical distributed multipole analysis with no charge transfer.[37, 38] Geometry optimization of the surfactant on a SWNT fragment was performed by randomly rotating the surfactant molecule, locating the surfactant center within 0 to 8 Å of the SWNT fragments' center in the convex region, and ensuring the initial nearest distance between the atoms would be limited to 1.5 and 5.0 Å. A total of 10,000 optimized configurations were collected and sorted by increasing EFP2 pair energies.

Essentially, the SWNT-surfactant pair was mapped onto the center of the larger SWNT molecule. After mapping, the short distance between surfactant atoms and the larger SWNT molecule allows the visual molecular dynamics (VMD) program to automatically assign these atoms as bonded. These bonded atoms are the results of using small EFP2 fragments to obtain an initial estimate of geometry optimization. The lowest fragment energy configuration that does not show these bonded atoms upon mapping was selected for further geometry optimization at the DFT-D3/BLYP/6-31G level. The final energies were then calculated using DFT-D3/BLYP/6-31++G(d,p) and interaction energies are calculated using Equation 3.

$$Binding\ Energy = E(SWNT-Surfactant) - E(SWNT) - E(Surfactant) \quad (3)$$

3. RESULTS AND DISCUSSION

3.1. Morphological and Chemical Characteristics

Chirality characterization of SG65 and SG76 SWNTs is reported in our previous work [30]; a chirality map showing major chiral indices for both samples is shown in Figure S1. Both the chiral SWNTs showed similar length as observed from the AFM imaging (Figure S2). The controlled sample preparation yielded a length range of 1.5–2.5 μm and 1.2–2.0 μm for SG65 and SG76, respectively. Since the length ranges of the tubes are similar between SG65

and SG76, we believe that length differences have played a minimal role in SWNT aggregation. Moreover, a recent study on the aggregation of MWNTs as a function of length further confirms the negligible role of length in smaller-diameter MWNT aggregation.[41] The pristine samples possess mean diameter distribution of 0.805±0.243 nm and 0.927±0.274 nm for SG65 and SG76, respectively (Figure S3); the diameter distribution is produced via NIR fluorescence spectroscopy as described earlier.[30] TEM micrographs in Figure 1 show SWNT physical morphology of pristine tubes and SWNTs with surfactant modification. Overall, both SG65 (top row: b–d) and SG76 (bottom row: f–h) show debundling and declustering in the presence of the surfactants when compared to the pristine cases (i.e., Figure 1a and 1d, respectively). Qualitatively, the packing density showed variation with relative increase in denseness (from left to right in Figure 1) as the surfactant changes from SDS to SDBS to SDOCO. The micrographs are similar to those found in previous literature on SWNTs modified with surfactants, polymeric surfactants, and biomacromolecules, showing debundling and declustering.[19, 42] Note that TEM micrographs are spot-specific, and thereby provide information on the qualitative bundling state of SWNTs in the presence of the surfactants.

Graphitic properties of SWNTs are evaluated with Raman spectroscopy as presented in Figure S4. The pristine SG65 and SG76 possess characteristic graphitic Raman signatures as represented by the defined peak at the ‘G’ band region of 1590 and 1595 cm^{-1}. Few defects are observed in the pristine SWNTs manifested with peaks at the defect ‘D’ band region of 1310 and 1330 cm^{-1}. The relative extent of any defects is estimated with a D/G ratio showing 0.24±0.01 and 0.12±0.01 for pristine SG65 and SG76, respectively. The Raman spectra for surfactant-modified cases showed similar peak responses near the G and D band regions, but with lower D/G ratios (Table S3). The decrease in D/G with surfactant most likely occurred due to electron shielding by the sorbed surfactant molecules. The literature has reported D/G ratios that are similar in magnitude showing a range of 0.05 to 0.21.[43] Similar shielding in Raman responses are consistently observed elsewhere.[44]

3.2. Electrokinetic Properties

EPM values for SWNTs are presented in Figures 2 (SG65) and S5 (SG76) for the considered range of NaCl and $CaCl_2$, respectively. Overall, the EPM profiles indicate the presence of negative surface potential for all electrolyte conditions and for both SG65 and SG76 with each of the anionic surfactants. There is a gradual decrease in the absolute value of EPM with the increase in electrolyte concentration. The presence of a negative surface charge attests to effective surfactant binding onto SWNT surfaces, similar to earlier observations.[45] In the presence of 1–100 mM NaCl, the absolute value of EPM for SG65 SWNTs decreased from $-(3.20\pm0.09)\times10^{-8}$ to $-(2.42\pm0.10)\times10^{-8}$, $-(3.88\pm0.09)\times10^{-8}$ to $-(3.17\pm0.02)\times10^{-8}$, and $-(3.44\pm0.13)\times10^{-8}$ to $-(2.74\pm0.00)\times10^{-8}$ $m^2V^{-1}S^{-1}$, for SDS, SDBS, and SDOCO, respectively (Figure 2a). SG76 SWNTs showed a similar trend in EPM, but with a magnitude enhancement for all surfactant cases (Figure S5a). The chiral difference thus has altered the electrokinetic properties, likely due to the higher interaction between the SG76 tubes and the anionic surfactants, as discussed in the modeling section. Moreover, the relative enhancement of surface potential with SDBS indicates higher surface coverage, likely the result of favorable π- π interaction between SWNTs and the aromatic

rings in the SDBS structure. Such sorption affinity for organic molecules with ring structures is observed in cases of humic substances [46] and other aromatics [47]. Both SDS and SDBS have showed EPM enhancement in the prior studies.[31, 32]

In presence of divalent Ca^{2+} ions, negative surface potential is observed on both SG65 (Figure 2b) and SG76 (Figure S5b) samples, but at relatively lower levels as compared to mono-valent Na^{+} cases. Similar electrokinetic behavior was observed for acid-functionalized SG65 and SG76 SWNTs earlier.[30] In the current case, the effect of chiral differences as well as surfactant structure was minimized, likely due to substantially higher electrostatic screening with Ca^{2+} cations.[48] Such higher electrostatic screening in the presence of divalent cations is similarly observed in earlier SWNT literature; SDBS-modified SWNTs and MWNTs showed similar decreases in absolute value of ζ potential from −27 to −10 and −34 to −14 mV, respectively, with an increase in divalent electrolyte concentration.[32]

3.3. Aggregation Behavior

Initial hydrodynamic radii of SG65 and SG76 SWNTs at DI water were measured at 138±12, 103±7, and 100±6 nm and 244±27, 199±15, and 201±18 nm for SDS, SDBS, and SDOCO modifications, respectively. Similar hydrodynamic radii of 117±8 and 208±11 nm for SG65 and SG76 SWNTs, respectively, were reported in our earlier work.[30] A relatively higher initial hydrodynamic radius of SG76 demonstrates higher tube-tube interaction propensity, compared to SG65 sample. Aggregation profiles for SG65 and SG76 SWNTs with NaCl electrolyte are shown in Figures 3(a–c) and S6(a–c), respectively. The attachment efficiencies (α) are estimated from initial aggregation rates using aggregation profiles and stability plots are shown in figure 4(a–b) with regards to NaCl concentration. All the stability profiles show classical Derjaguin-Landau-Verwey-Overbeek (DLVO) type behavior. The key finding from the aggregation kinetics study is the ability of SDBS to stabilize SWNTs relative to SDS and SDOCO, as indicated by the 170 mM NaCl value, the critical coagulation concentration (CCC) for SG65 SWNT. However, the change in chiral enrichment to the SG76 sample resulted in compromised stability, as reflected by a CCC value of 44 mM NaCl. This is evident from Figure 4(a–b), where ½ to 1 log-unit leftward shift is observed for the most stable case (i.e., SDBS), as the tube chirality changed from (6,5) to (7,6). The CCC values of SDS and SDOCO modified SG65 and SG76 were estimated as 18 and 41 mM NaCl and 29 and 34 mM NaCl, respectively. The findings demonstrate that though SWNT stabilization can be surfactant-dependent, the role of surfactant type diminishes with the change in chirality of semiconducting tubes. Previously, a wide range of CCC values were reported: 121 mM to 870 mM NaCl for 0.0005 to 0.05% SDS modification[31] and 90 mM NaCl for SDBS modification[32]. Covalent functionalization, however, showed lower effectiveness in stabilizing SWNTs as reflected by CCC values of 37 mM and 20 mM NaCl for the acid etching and mechnochemical processes, respectively.[28, 29] However, the chiral specificity of the SWNTs in these studies was unknown. The only study to date reporting the role of chirality is our previous publication where SG76 showed a significantly lower CCC value compared to that of SG65: a CCC of 13 and 96 mM NaCl for SG76 and SG65, respectively.[30]

The other key finding from the aggregation kinetics study is the significant effect of $CaCl_2$ in minimizing the effects of chirality change and surfactant differences on SWNT aggregation. The aggregation behavior showed similar DLVO type behavior for both SG65 and SG76, however, with at least one logarithmic left-shift (Figure 4c–d). The attachment efficiencies are similarly estimated from aggregation rates using aggregation profiles presented in Figures S7(a–c) and S8(a–c). The presence of $CaCl_2$ overshadowed the surfactant stabilization and caused overlapping of the stability profiles of SWNTs, yielding CCC values of 0.7, 2.2, and 1.3 mM $CaCl_2$ with SDS, SDBS, and SDOCO modification of SG65, respectively. In addition, change in chirality also did not result in significant differences in the CCC values; the values were estimated as 1.4, 1.7, and 0.7 mM $CaCl_2$ for SDS, SDBS, and SDOCO modifications of SG76. Recent studies employing SDBS and SDS stabilization reported similar CCC values of 0.82 and 2.52 mM $CaCl_2$, respectively.[31, 32] Covalent functionalization also showed consistent range of CCC values; i.e., 0.2 mM and 2.0 mM $CaCl_2$ for acid etching and mechnochemical processes, respectively.[28, 29] It is interesting to note that presence of divalent cations can not only suppress the role of surface functionality but can also reduce the effect of chiral differences on aggregation, as evidenced by reported CCC values of 2.8 and 0.6 mM $CaCl_2$ for SG65 and SG76, respectively.[30]

3.4. Molecular Modeling of SWNT-Surfactant Interaction

Figure 5 shows the optimized configuration of the negatively charged surfactants on the SWNT and the interaction energies. The optimum SDBS configuration has the face of the aromatic ring parallel to the surface of the SWNT. The SDOCO has the concave section of the surfactant oriented along the surface of the SWNT with the methyl groups oriented away from the tubes. The axis of SDS appears to be parallel to that of the SWNT. All interaction energies between the surfactant and the SWNTs are favorable, confirming that the surfactants would be bound to the surfaces of the SWNT. The lowest interaction energy is for the SDBS surfactant, which indicates the smallest surface footprint for dispersion interactions. More favorable interaction energies are calculated for SG76 compared to SG65 because of the larger radius of SG76. This finding signifies that a higher binding preference is expected for SG76 as compared to SG65, as consistently observed in higher EPM values.

3.5. Aggregation Mechanisms

SWNTs are known to possess high aggregation propensity due to substantial van der Waals interaction. Such attractive interaction is also influenced by the atomic arrangement, (i.e., the chirality) of the SWNTs. As previously observed, SWNT aggregation is substantially increased with the increase in diameter for similar chiral-angled tubes; i.e., SG76 is observed to have higher aggregation propensity compared to SG65 under environmentally relevant electrolyte conditions.[30] The key mechanism is identified as increased Hamaker constant for larger diameter SG76, resulting in enhanced van der Waals interaction, thus dominating the aggregation behavior.[30] In this study, aggregation behavior undergoes further differences due to the change in surface functionalization; i.e., non-covalent surfactant modification instead of covalent carboxylation. The SDBS molecular structure has likely played an important role to provide higher stability to SWNTs. The structural difference between SDS and SDBS is essentially an added aromatic ring for the latter; in

contrast, SDOCO possesses both a higher molecular weight as well as a unique structural configuration (Table S1). The presence of the aromatic ring in SDBS has likely caused increased affinity of the surfactant molecules toward SWNTs, as compared to the linear chained SDS. SDOCO molecules with cyclic organic features likely possessed hydrophobic interaction forces that resulted in a higher footprint on SWNT surfaces, as observed from relatively higher interaction energies. The adsorbed SDS, SDBS, and SDOCO have resulted in surface charge incorporation and the increased electrostatic stability of the SWNTs. Since aggregation is an interplay between electrostatic repulsion and van der Waals attraction, the higher attractive forces imparted by larger diameter SG76 tubes have largely masked the stabilization effects provided by SDBS. Similarly, higher electrostatic screening with Ca^{2+} cations caused a masking effect for the adsorbed surfactants, resulting in reduced stability in presence of all three surfactants (Figure 4c–d). Molecular modeling is thus performed to further probe aggregation mechanisms for non-covalent surface modification.

Figure 5 evinces that the structural variation between surfactants resulted in the greatly varied surface footprint of the molecules, as discussed earlier. The interaction energies between SDS, SDBS, and SDOCO show higher favorability for SG76, compared to SG65; i.e., −42.7, −35.7, and −40.8 kcal/mol, compared to −39.6, −33.7, −38.3 kcal/mol, respectively. The higher interaction energy values of SG76 indicate a potentially higher surface coverage for all surfactants, which is consistently demonstrated by relatively higher EPM values for this chirality (Figure S5). Interestingly, the SDBS cases have the lowest interaction energies as compared to SDS and SDOCO. At first glance, this outcome appears to be contradictory to the aggregation and SDBS-SWNT association findings—where SDBS is observed as the strongest stability enhancer with a strong association with the tubes (TEM). However, the molecular orientation differences can explain both the interaction energy estimations as well as explain the aggregation propensity trend. Geometry optimization shows that linear chain SDS molecules attain parallel configuration with SG65 and SG76 principal axes. Such a configuration not only indicates a large molecular footprint for the SDS—and thereby lower surface coverage—but also explains the relatively higher interaction energy results emanating from the interaction of a larger number of surfactant atoms with the carbon atoms on the SWNTs. In comparison, the optimized configuration for SDBS modification shows close proximity of the aromatic ring and a wide angular deviation of the rest of the surfactant chain from SWNT surfaces. It similarly explains the relatively lower interaction energy estimation through large distance-separation of the aliphatic chain from SWNT carbon atoms. Such an orientation of SDBS molecules likely has resulted in the smaller footprint and thereby an increased surface coverage, as observed from the EPM values (Figures 2 and S5), TEM (Figure 1), and the enhanced stability of this surfactant (Figure 4). Finally, the SDOCO surfactant with a ‘cupped’ structure showed casping of SWNT around its diameter, thus creating a similarly large molecular footprint. Such an orientation resulted in a high level of atom proximity to the SWNT carbon atoms and thus generated a relatively higher interaction energy value. The key manifestation of stability enhancement by SDBS is thus likely to have resulted from the greater surfactant density on SWNT surfaces as well as from the steric contribution of the outward extended chain of the SDBS—a set of conditions unique to this particular surfactant.

3.6. Role of SRHA on SWNT Aggregation

The initial aggregation rates (Table S4) of SDS, SDBS, and SDOCO stabilized SG65 and SG76 SWNTs with and without the presence of SRHA under a 10 mM ionic strength electrolyte condition are estimated from corresponding aggregation profiles. Overall, the rate of aggregation (nm/s) of SWNTs, irrespective of any specific surfactant, undergoes substantial decrease, i.e., 64.7 to 99.4%, for all cases with the addition of SRHA (Figure S9). For SG65, the aggregation rates decreased with SRHA in 10 mM NaCl condition from 0.148±0.019 to 0.030±0.002, 0.061±0.004 to 0.015±0.012, and 0.101±0.008 to 0.017±0.013 nm/s for SDS, SDBS, and SDOCO, respectively. Similar stability increase is observed in case of SG76. Moreover, the presence of 1 mM Ca^{2+} cations increased the overall aggregation rates, yet shows a substantial decrease with SRHA addition for all surfactant cases.

Such increased stability with SRHA is most likely the result of surfactant molecule replacement with larger SRHA macromolecules. The average SRHA molecular weight is reported to be approximately 1,490 Da, as reported by International Humic Substances Society, which is at least three times higher than that of all three surfactants used. It is well known in the literature that higher molecular weight macromolecules preferentially replace smaller molecular weight surfactants.[49] Thus SDS, SDBS, and SDOCO molecules are likely replaced with SRHA, providing elctrosteric stabilization to both SG65 and SG76 and diminishing surfactant-specific response for aggregation. Such enhanced stabilization is observed earlier for both SWNTs and MWNTs.[32] Fullerenes also showed similar stabilization with NOM.[50]

4. CONCLUSIONS

SWNTs, upon release to the aquatic environment, will interact with surfactant molecules. SWNT aggregation will thus be influenced by the type of surfactant molecules as well as by their chiral identity. Results indicate that change in chirality from (6,5) to (7,6), can influence CCC values; however, the influence of chirality is also dependent on surfactant structure, which controls surfactant configuration on tube surfaces and subsequent SWNT aggregation. SDBS surfactant has shown to play an insignificant role in SWNT stabilization, while chirality change dominated the aggregation behavior, as shown by nearly a ½ log unit leftward shift in CCC for (7,6) chirality. In contrast, SDS and SDOCO are effective in stabilization of SWNTs and minimize the role of chirality changes, as shown by the narrow differences between the CCC values of the two chiral tubes. In the case of the divalent electrolyte Ca^{2+}, the surfactant stabilization is suppressed and role of chirality is also diminished, as indicated by minor differences in CCC values for all cases examined. Results further show that NOMs, such as SRHA, significantly reduce aggregation rate and enhance SWNT stability in typical aquatic environments. Thus SWNT aggregation behavior in an aqueous system will likely be dominated by the chiral identity of the tubes as well as by the structure of surfactant coating. Divalent electrolytes will likely diminish stabilization effects while NOMs will overcome aggregation propensity and stabilize SWNTs in most aquatic environments.

Supplementary Material

Refer to Web version on PubMed Central for supplementary material.

Acknowledgments

Funding was provided by the National Science Foundation (CBET 0933484) and National Institute of Health (R01HL114907). We are grateful to Dr. Haijun Qian of Clemson Microscopy Center for his kind assistance in TEM imaging.

References

1. Iijima S, Ichihashi T. Single-Shell Carbon Nanotubes of 1-nm Diameter. Nature. 1993; 363:603–5.
2. Saito, R.; Dresselhaus, G.; Dresselhaus, MS. Physical properties of carbon nanotubes. Imperial college press; London: 1998.
3. Weisman, RB. Contemporary Concepts of Condensed Matter Science. Saito, S.; Zettl, A., editors. Elsevier; 2008. p. 109-33.
4. Baughman RH, Zakhidov AA, de Heer WA. Carbon nanotubes - the route toward applications. Science. 2002; 297(5582):787–92. [PubMed: 12161643]
5. Chen KJ, Nair N, Strano MS, Braatz RD. Identification of chirality-dependent adsorption kinetics in single-walled carbon nanotube reaction networks. J Comput Theor Nanosci. 2010; 7(12):2581–5.
6. Hirsch A. Functionalization of Single-Walled Carbon Nanotubes. Angew Chem Int Ed. 2002; 41(11):1853–9.
7. Bahr JL, Tour JM. Covalent Chemistry of Single-wall Carbon Nanotubes. J Mater Chem. 2002; 12(7):1952–8.
8. Haggenmueller R, Rahatekar SS, Fagan JA, Chun J, Becker ML, Naik RR, et al. Comparison of the Quality of Aqueous Dispersions of Single Wall Carbon Nanotubes Using Surfactants and Biomolecules. Langmuir. 2008; 24(9):5070–8. [PubMed: 18442227]
9. Biswas C, Lee YH. Graphene Versus Carbon Nanotubes in Electronic Devices. Adv Funct Mater. 2011; 21(20):3806–26.
10. Villa CH, Dao T, Ahearn I, Fehrenbacher N, Casey E, Rey DA, et al. Single-Walled Carbon Nanotubes Deliver Peptide Antigen into Dendritic Cells and Enhance IgG Responses to Tumor-Associated Antigens. ACS Nano. 2011; 5(7):5300–11. [PubMed: 21682329]
11. Cha T-G, Baker BA, Sauffer MD, Salgado J, Jaroch D, Rickus JL, et al. Optical Nanosensor Architecture for Cell-Signaling Molecules Using DNA Aptamer-Coated Carbon Nanotubes. ACS Nano. 2011; 5(5):4236–44. [PubMed: 21520951]
12. Mauter MS, Elimelech M. Environmental Applications of Carbon-Based Nanomaterials. Environ Sci Technol. 2008; 42(16):5843–59. [PubMed: 18767635]
13. Shim BS, Zhu J, Jan E, Critchley K, Ho S, Podsiadlo P, et al. Multiparameter Structural Optimization of Single-Walled Carbon Nanotube Composites: Toward Record Strength, Stiffness, and Toughness. ACS Nano. 2009; 3(7):1711–22. [PubMed: 19591447]
14. Lam CW, James JT, McCluskey R, Arepalli S, Hunter RL. A Review of Carbon Nanotube Toxicity and Assessment of Potential Occupational and Environmental Health Risks. Crit Rev Toxicol. 2006; 36(3):189–217. [PubMed: 16686422]
15. Petosa AR, Jaisi DP, Quevedo IR, Elimelech M, Tufenkji N. Aggregation and Deposition of Engineered Nanomaterials in Aquatic Environments: Role of Physicochemical Interactions. Environ Sci Technol. 2010; 44(17):6532–49. [PubMed: 20687602]
16. Liu J, Rinzler AG, Dai H, Hafner JH, Bradley RK, Boul PJ, et al. Fullerene Pipes. Science. 1998; 280(5367):1253–6. [PubMed: 9596576]
17. Chen RJ, Zhang Y, Wang D, Dai H. Noncovalent Sidewall Functionalization of Single-Walled Carbon Nanotubes for Protein Immobilization. J Am Chem Soc. 2001; 123(16):3838–9. [PubMed: 11457124]

18. Moore VC, Strano MS, Haroz EH, Hauge RH, Smalley RE, Schmidt J, et al. Individually Suspended Single-Walled Carbon Nanotubes in Various Surfactants. Nano Lett. 2003; 3(10): 1379–82.
19. Liu Y, Gao L, Zheng S, Wang Y, Sun J, Kajiura H, et al. Debundling of Single-Walled Carbon Nanotubes by Using Natural Polyelectrolytes. Nanotechnology. 2007; 18(36):365702.
20. Alpatova AL, Shan W, Babica P, Upham BL, Rogensues AR, Masten SJ, et al. Single-walled carbon nanotubes dispersed in aqueous media via non-covalent functionalization: Effect of dispersant on the stability, cytotoxicity, and epigenetic toxicity of nanotube suspensions. Water Res. 2010; 44(2):505–20. [PubMed: 19945136]
21. Zou J, Khondaker SI, Huo Q, Zhai L. A General Strategy to Disperse and Functionalize Carbon Nanotubes Using Conjugated Block Copolymers. Adv Funct Mater. 2009; 19(3):479–83.
22. Kim KK, Yoon SM, Choi JY, Lee J, Kim BK, Kim JM, et al. Design of Dispersants for the Dispersion of Carbon Nanotubes in an Organic Solvent. Adv Funct Mater. 2007; 17(11):1775–83.
23. Vaisman L, Wagner HD, Marom G. The Role of Surfactants in Dispersion of Carbon Nanotubes. Adv Colloid Interface Sci. 2006; 128–130:37–46.
24. Aich N, Flora JRV, Saleh NB. Preparation and Characterization of Stable Aqueous Higher-Order Fullerenes. Nanotechnology. 2012; 23(5):055705. [PubMed: 22236869]
25. Chen KL, Smith BA, Ball WP, Fairbrother DH. Assessing the colloidal properties of engineered nanoparticles in water: case studies from fullerene C60 nanoparticles and carbon nanotubes. Environ Chem. 2010; 7(1):10–27.
26. Saleh NB, Pfefferle LD, Elimelech M. Aggregation Kinetics of Multiwalled Carbon Nanotubes in Aquatic Systems: Measurements and Environmental Implications. Environ Sci Technol. 2008; 42(21):7963–9. [PubMed: 19031888]
27. Yi P, Chen KL. Influence of Surface Oxidation on the Aggregation and Deposition Kinetics of Multiwalled Carbon Nanotubes in Monovalent and Divalent Electrolytes. Langmuir. 2011; 27(7): 3588–99. [PubMed: 21355574]
28. Saleh NB, Pfefferle LD, Elimelech M. Influence of Biomacromolecules and Humic Acid on the Aggregation Kinetics of Single-Walled Carbon Nanotubes. Environ Sci Technol. 2010; 44(7): 2412–8. [PubMed: 20184360]
29. Sano M, Okamura J, Shinkai S. Colloidal nature of single-walled carbon nanotubes in electrolyte solution: The Schulze-Hardy rule. Langmuir. 2001; 17(22):7172–3.
30. Khan IA, Afrooz ARMN, Flora JRV, Schierz PA, Ferguson PL, Sabo-Attwood T, et al. Chirality Affects Aggregation Kinetics of Single-Walled Carbon Nanotubes. Environ Sci Technol. 2013; 47(4):1844–52. [PubMed: 23343128]
31. Bouchard D, Zhang W, Powell T, Rattanaudompol Us. Aggregation Kinetics and Transport of Single-Walled Carbon Nanotubes at Low Surfactant Concentrations. Environ Sci Technol. 2012; 46(8):4458–65. [PubMed: 22443301]
32. Ju L, Zhang W, Wang X, Hu J, Zhang Y. Aggregation Kinetics of SDBS-Dispersed Carbon Nanotubes in Different Aqueous Suspensions. Colloids Surf Physicochem Eng Aspects. 2012; 409(0):159–66.
33. Zaib Q, Khan IA, Saleh NB, Flora JRV, Park Y-G, Yoon Y. Removal of Bisphenol A and 17 β-Estradiol by Single-Walled Carbon Nanotubes in Aqueous Solution: Adsorption and Molecular Modeling. Water Air Soil Pollut. 2012; 223(6):3281–93.
34. Grimme S, Antony J, Ehrlich S, Krieg H. A Consistent and Accurate *ab initio* Parametrization of Density Functional Dispersion Correction (DFT-D) for the 94 Elements H-Pu. J Chem Phys. 2010; 132(15):154104. [PubMed: 20423165]
35. Ufimtsev IS, Martinez TJ. Quantum Chemistry on Graphical Processing Units. 3. Analytical Energy Gradients, Geometry Optimization, and First Principles Molecular Dynamics. J Chem Theory Comput. 2009; 5(10):2619–28. [PubMed: 26631777]
36. Gordon, MS.; Schmidt, MW. Theory and Applications of Computational Chemistry. Clifford, ED.; Gernot, F.; Kwang, SK.; Gustavo, ES., editors. Elsevier; Amsterdam: 2005. p. 1167-89.
37. Gordon, MS.; Slipchenko, L.; Li, H.; Jensen, JH. Annual Reports in Computational Chemistry. Spellmeyer, DC.; Wheeler, R., editors. Elsevier; 2007. p. 177-93.

38. Schmidt MW, Baldridge KK, Boatz JA, Elbert ST, Gordon MS, Jensen JH, et al. General Atomic and Molecular Electronic-Structure System. J Comput Chem. 1993; 14(11):1347–63.

39. Smith T, Slipchenko LV, Gordon MS. Modeling π-π Interactions with the Effective Fragment Potential Method: The Benzene Dimer and Substituents. J Phys Chem A. 2008; 112(23):5286–94. [PubMed: 18476681]

40. Bode BM, Gordon MS. Macmolplt: A Graphical User Interface for GAMESS. J Mol Graphics Model. 1998; 16(3):133–8.

41. Ntim SA, Sae-Khow O, Desai C, Witzmann FA, Mitra S. Size dependent aqueous dispersibility of carboxylated multiwall carbon nanotubes. Journal of Environmental Monitoring. 2012; 14(10): 2772–9. [PubMed: 22972403]

42. Furtado CA, Kim UJ, Gutierrez HR, Pan L, Dickey EC, Eklund PC. Debundling and Dissolution of Single-Walled Carbon Nanotubes in Amide Solvents. J Am Chem Soc. 2004; 126(19):6095–105. [PubMed: 15137775]

43. Shen K, Curran S, Xu HF, Rogelj S, Jiang YB, Dewald J, et al. Single-Walled Carbon Nanotube Purification, Pelletization, and Surfactant-Assisted Dispersion: A Combined TEM and Resonant Micro-Raman Spectroscopy Study. J Phys Chem B. 2005; 109(10):4455–63. [PubMed: 16851517]

44. Chusuei, CC.; Wayu, M. Electronic Properties of Carbon Nanotubes. Marulanda, JM., editor. InTech; 2011.

45. White B, Banerjee S, O'Brien S, Turro NJ, Herman IP. Zeta-Potential Measurements of Surfactant-Wrapped Individual Single-Walled Carbon Nanotubes. Journal of Physical Chemistry C. 2007; 111(37):13684–90.

46. Wang X, Tao S, Xing B. Sorption and Competition of Aromatic Compounds and Humic Acid on Multiwalled Carbon Nanotubes. Environ Sci Technol. 2009; 43(16):6214–9. [PubMed: 19746716]

47. Chin YP, Aiken GR, Danielsen KM. Binding of Pyrene to Aquatic and Commercial Humic Substances: The role of molecular weight and aromaticity. Environ Sci Technol. 1997; 31(6): 1630–5.

48. Schwyzer I, Kaegi R, Sigg L, Nowack B. Colloidal stability of suspended and agglomerate structures of settled carbon nanotubes in different aqueous matrices. Water Res. 2013; 47(12): 3910–20. [PubMed: 23582307]

49. Xu H, Schlenoff JB. Kinetics, Isotherms, and Competition in Polymer Adsorption Using the Quartz-Crystal Microbalance. Langmuir. 1994; 10(1):241–5.

50. Zhang W, Rattanaudompol Us, Li H, Bouchard D. Effects of humic and fulvic acids on aggregation of aqueous nC60 nanoparticles. Water Res. 2013; 47(5):1793–802. [PubMed: 23374256]

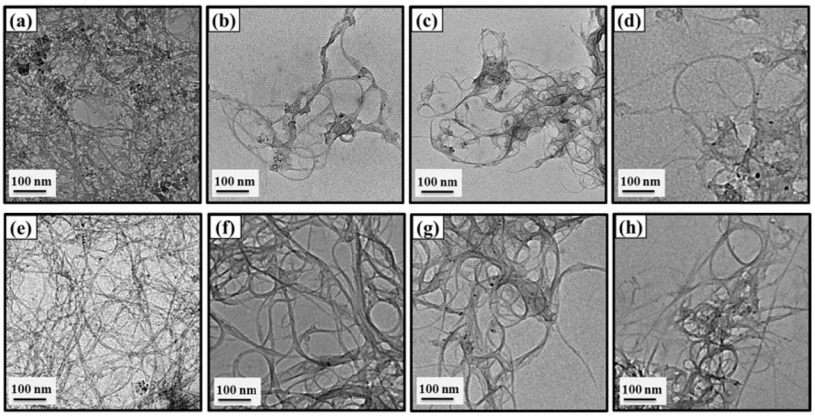

Figure 1.

High resolution TEM micrographs of SWNTs: top row for SG65 and bottom row for SG76 SWNTs. Pristine, SDS, SDBS, and SDOCO functionalized SWNTs are placed from left to right, i.e., (a) SG65-Pristine, (b) SG65-SDS, (c) SG65-SDBS, (d) SG65-SDOCO, (e) SG76-Pristine, (f) SG76-SDS, (g) SG76-SDBS, and (h) SG76-SDOCO. Functionalized SWNTs are debundled and declustered in comparison to respective pristine tubes.

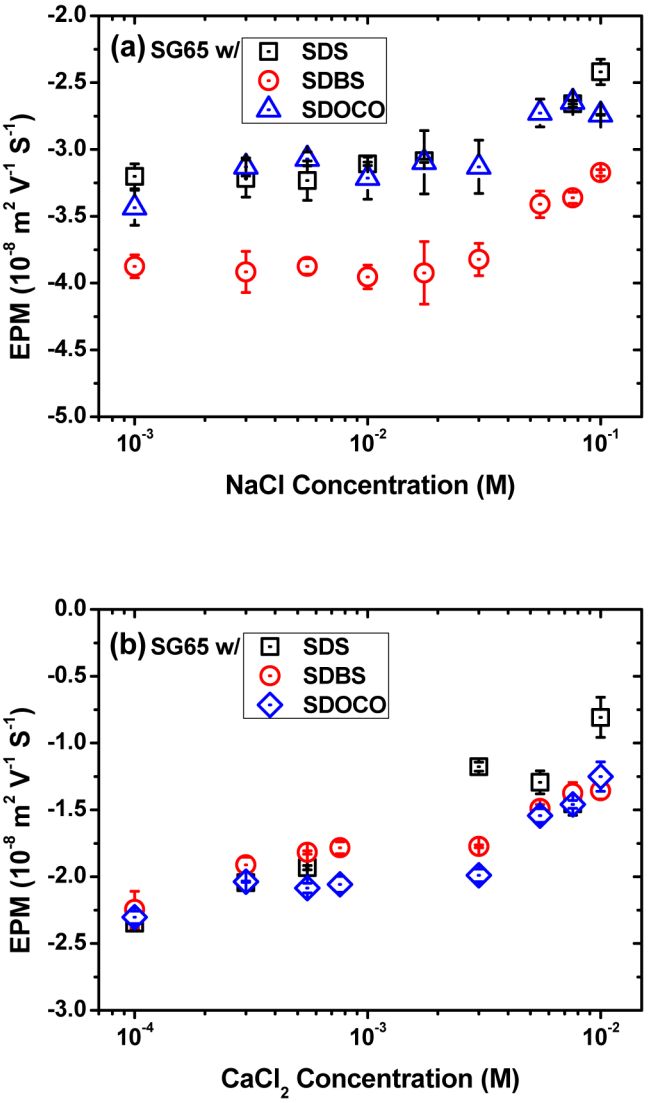

Figure 2.

EPM of SG65 SWNTs as a function of (a) NaCl and (b) $CaCl_2$ salt concentration. At least three separate experiments were performed for each condition and data presented here represent the mean of three independent experiments with one standard deviation. Measurements were carried out at a pH of ~6.5 and a temperature of 20±0.5 °C.

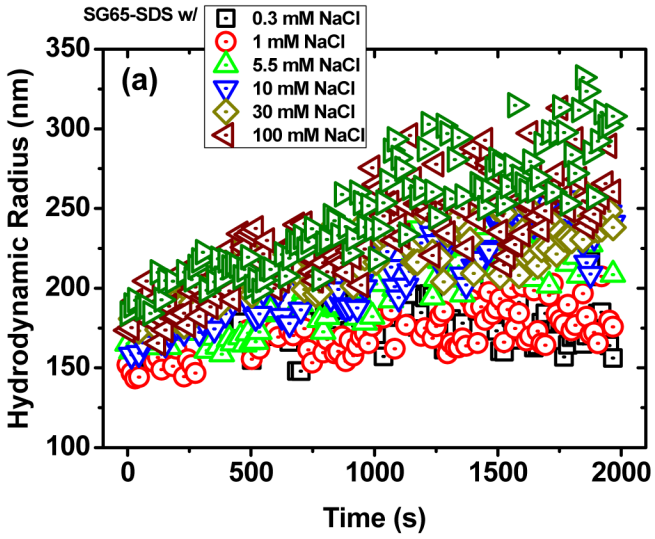

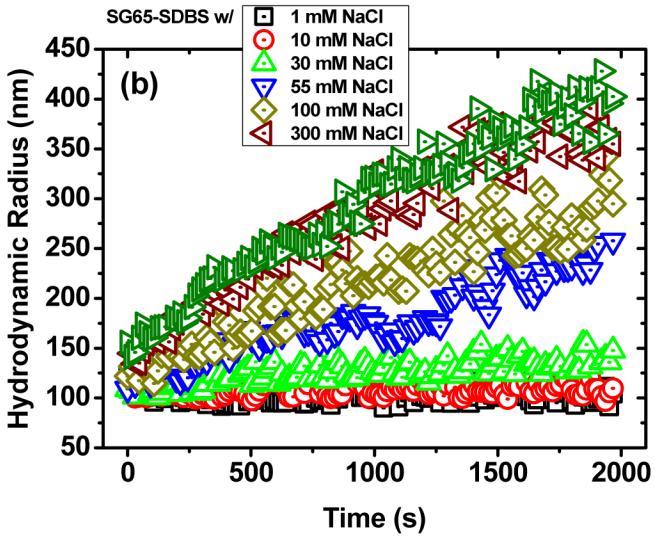

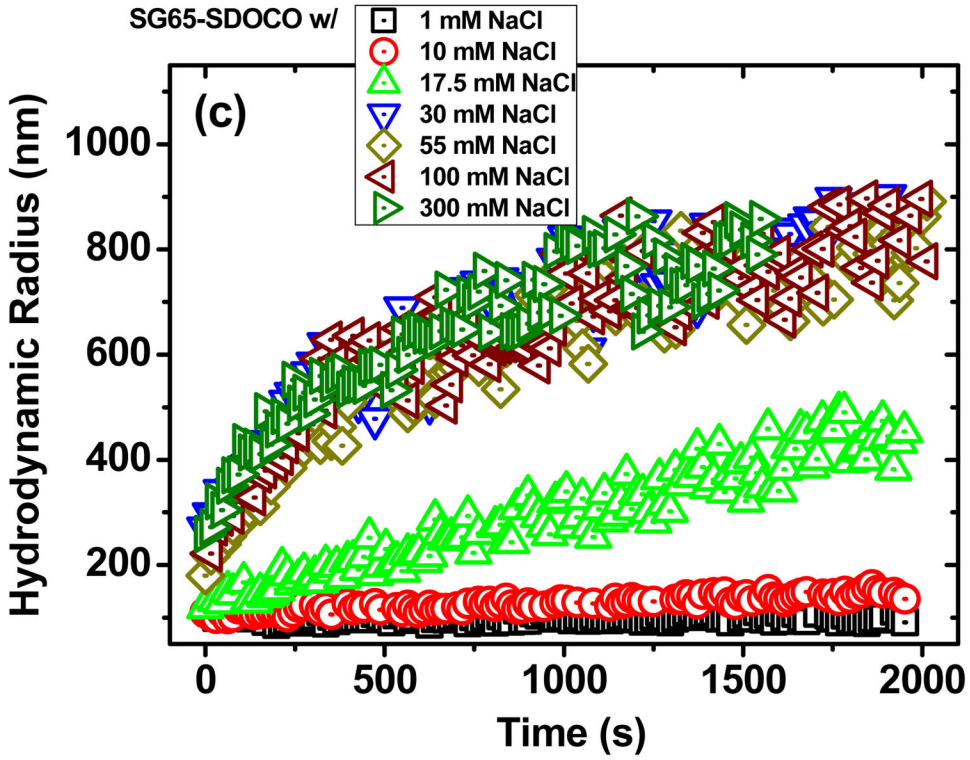

Figure 3.

Aggregation profiles of (a) SDS, (b) SDBS, and (c) SDOCO modified SG65 SWNTs under a wide range of NaCl concentration. Aggregation experiments were conducted at a temperature of 20±0.5 °C and at least 2 duplicate samples were tested to obtain significant reproducibility.

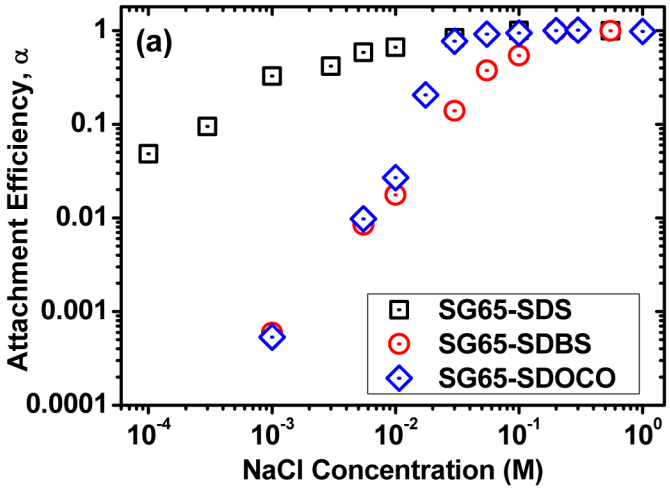

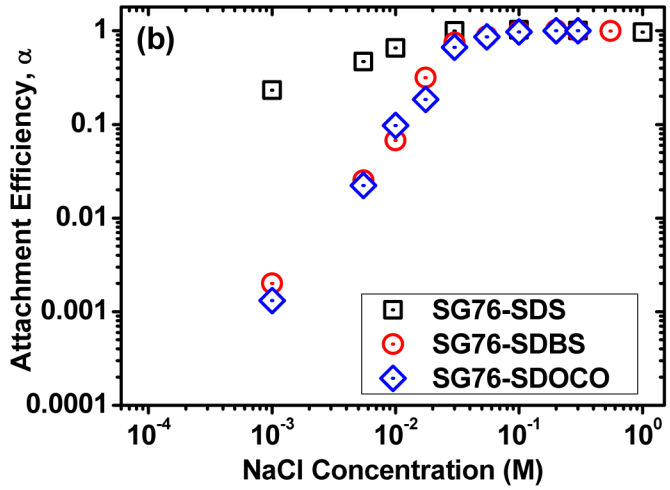

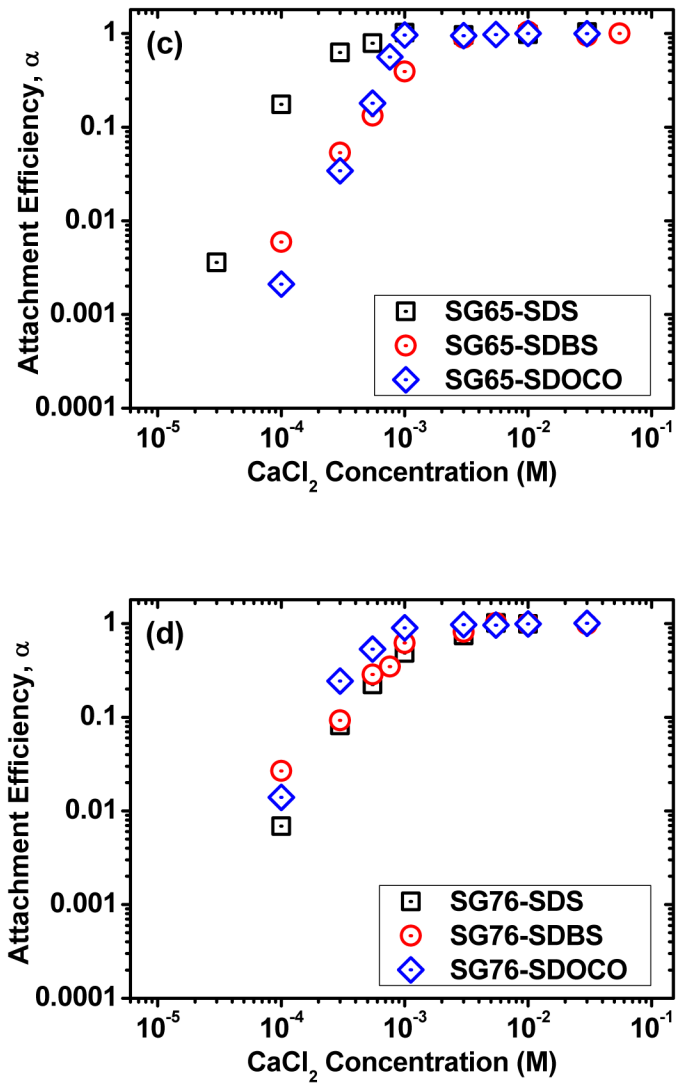

Figure 4.

Stability plots of (a) SG65 and (b) SG76 SWNTs as a function of NaCl salt concentration, and (c) SG65 and (d) SG76 SWNTs as a function of $CaCl_2$ salt concentration. The attachment efficiencies are calculated by normalizing the actual aggregation rate with the favorable (fast) aggregation rate. All the rates are calculated from corresponding aggregation profiles: Figures S6 (SG65-NaCl), S7 (SG76-NaCl), S8 (SG65-$CaCl_2$) and S9 (SG76-$CaCl_2$), respectively. Aggregation experiments were conducted at a temperature of 20±0.5 °C.

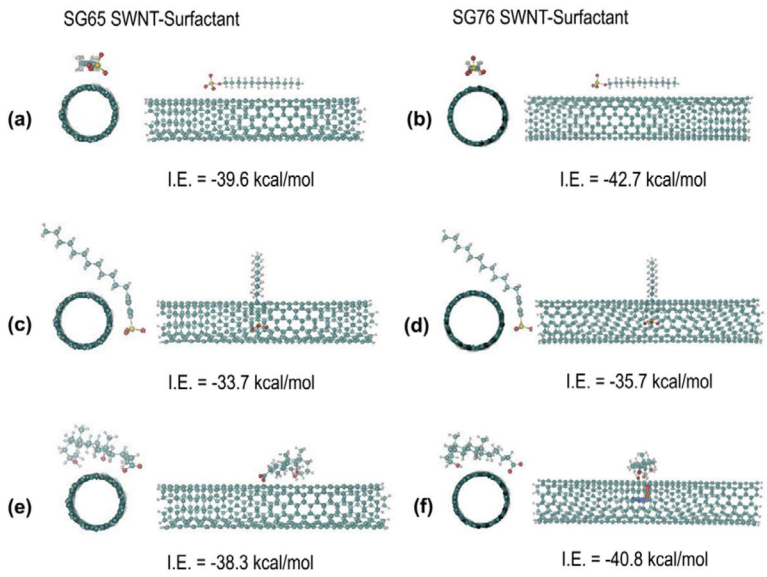

Figure 5.

Front and side views of representative gas phase optimized geometries for surfactants adsorbed on SWNTs. Left column is for SG65 and right column is for SG76 SWNTs. Top to bottom: SWNTs with (a–b) SDS, (c–d) SDBS, and (e–f) SDOCO surfactants. The interaction energy (I.E.) for each SWNT-surfactant is shown below the side view snapshot for each case. The I.E. of (a) SG65-SDS, (b) SG76-SDS, (c) SG65-SDBS, (d) SG76-SDBS, (e) SG65-SDOCO, and (f) SG76-SDOCO are −39.6, −42.7, −33.7, −35.7, −38.3, and −40.8 kcal/mol, respectively.